J. KAU: Mar. Sci., **vol. 12,** *Special Issue,* pp. 101-113 (1421 A.H. / 2001 A.D.)

Late Quaternary Climate Records from the Northern Red Sea: Results on Gravity Cores Retrieved during the R/V METEOR Cruise M44/3

HELGE W. ARZ[1], JÜRGEN PÄTZOLD[1]
MUSTAFA O. MOAMMAR[2], and URSULA RÖHL[1]
[1]*Fachbereich Geowissenschaften, Universität Bremen, Klagenfurter Str. D-28359, Bremen, Germany; and*
[2]*Faculty of Marine Science,King Abdulaziz University, P.O. Box 15389, Jeddah 21444, Saudi Arabia*

ABSTRACT. We present high-resolution marine paleoclimate records obtained from sediment cores retrieved along three profiles extending from the Saudi Arabian coast to the central axis of the northern Red Sea during R/V METEOR cruise M44/3 in spring 1999. Because of its restricted, desert surrounded location, the northern Red Sea suffered extreme oceanographic changes in the past, resulting in an amplification of paleoclimatic signals in the marine sediments. The continuous deposition of wind-blown and fluvially transported terrigenous material provides a high temporal resolution of changes in the aridity of the adjacent continents. Such changes are documented by independent indicators, *i.e.*, variations of the bulk-sediment chemistry (Fe- and Ti-content determined by profiling XRF measurements) and magnetic susceptibility. Synchronously, changes in the marine environment are reflected by variations in the carbonate content (*i.e.*, Ca- and Sr-intensities). Our records provide evidence of a strong coupling of both aridity changes in the Near East and paleoceanographic conditions in the northern Red Sea to global climate and sea level changes as well as variations in the monsoonal system.

Introduction

As a desert-enclosed basin with a reduced exchange of water with the Indian Ocean through the Strait of Bab el Mandeb, the Red Sea shows strong S-N gradients in sea surface temperature, salinity, and primary production (*e.g.*, Edwards, 1986). Due to its restricted location, the Red Sea suffered extreme oceanographic changes in the past and therefore amplified global and regional climatic signals are expected to be recorded in the sedimentary deposits of the sea floor. During the Last Glacial Maximum (LGM) for example, when the global sea level was about 120 m lower than today, water exchange with the Indian Ocean was substantially reduced and surface salinities increased in the Red Sea by as much as 16‰ (Hemleben *et al*., 1996). For most of the planktic organisms the salinity tolerance was exceeded during this interval and anorganic carbonate precipitation took place. In the deep sea sediments, this interval is documented by a so called "aplanktic zone" and a lithified carbonate layer (Almogi-Labin *et al.*, 1998; Brachert, 1995; Locke & Thunell, 1988; Milliman *et al*., 1969 and Winter *et al*., 1983). Although the global

Correspondence to:
Helge W. Arz, e-mail: helge.arz@uni-bremen.de, Fax: (++49) 421 218 3116.

sea level change of the past glacial/interglacial periods is one of the major controlling factors on the Red Sea marine environment (*e.g.*, Gvirtzman *et al*., 1992; Hemleben *et al*., 1996), variations in the African-Asian monsoonal system and teleconnective atmospheric processes from the Atlantic sector clearly affect the Red Sea and especially the northern Red Sea region (Almogi-Labin *et al*., 1998; Hemleben *et al*., 1996 and Schmelzer *et al.,* 1998).

The goal of our paleoclimatologic studies is to reconstruct and distinguish the effects of climate and sea level changes on the terrigenous sediment input, the surface ocean circulation and productivity, and also deep-water formation in the northern Red Sea on different time scales (Holocene, Marine Isotope Stage 2-4, glacial/interglacial cycles). Here, we present first results of different core logging methods, which we applied on the gravity cores retrieved from the northern Red Sea during the R/V METEOR cruise M44/3 in spring 1999 (Pätzold and cruise participants, 1999).

Climate and Ocean Circulation

The Red Sea area is a desert-enclosed, relative young rift basin located within the African-Asian arid belt. Climatically, the region is dominated by the descending branch of the northern Hadley-cell (Barry and Chorley, 1998). In the northern Red Sea, winds blow year round from NW to NNW along the Red Sea axial through, while south of 19ºN seasonally changing monsoonal winds can be found blowing from NNW in summer and much stronger from SSE in winter (Patzert, 1972). Precipitation and runoff are negligible and besides slightly increased precipitation in the north due to moisture transport from the Mediterranean area (2.5 cm/a), excess evaporation is dominating the Red Sea (ca. 200 cm/a; Morcos, 1970).

In previous works (Cember, 1988; Eshel *et al*., 1994; Patzert, 1972 and Tragou & Garrett, 1997) and recently in a comprehensive numerical model (Eshel and Naik, 1997) it was shown that the surface circulation in the Red Sea is dominated by northward-flowing, density driven boundary currents with only secondary wind forcing. Relatively fresh and nutrient rich waters enter the Red Sea through the shallow Strait of Bab el Mandeb from the Gulf of Aden. Due to strong evaporation and cooling, the northward-flowing surface waters are getting continuously denser. Forced by the large-scale meridional sea surface tilt, they end up in the northern Red Sea, where southward-flowing intermediate and deep water are initiated. Intermediate water formation occurs at the collision site of the Eastern and Western Boundary Currents (Fig. 1) and is dependent on the thermohaline preconditioning of the northward-flowing upper-layer water over several years and the interaction with the dense subsurface waters leaving the Gulfs of Suez and Aqaba (Cember, 1988 and Eshel & Naik, 1997). Deep-water formation occurs in the center of the northern basin cyclonic gyre and is of episodic nature related to intense atmospheric events (Fig. 1) (Eshel & Naik, 1997 and Woelk & Quadfasel, 1996).

Material and Methods

During the R/V METEOR cruise M44/3 we sampled seafloor sediments at 19 stations in the northern Red Sea by means of multicorer and gravity corer from water depths between 587 and 1533 m. All details are given in the station list of the cruise report (Pätzold and Cruise participants, 1999). Along three profiles extending from the Saudi Arabian coast to the central axis of the northern Red Sea altogether 18 gravity cores were recovered of which we selected four cores, GeoB 5824-3, 5833-2, 5840-2, and 5844-2, for our investigations (Table 1, Fig. 1). All cores were cut into an archive and work half. The archive half was used for core description, smear slide sampling, core photography, color scanning and other profiling measurements. The work half is designated for detailed subsampling.

Core Description, Smear Slides and Sediment Color

In order to supplement the macroscopic core description, a smear slide analysis was carried out. Smear slides were taken from all representative lithologies and were examined using a light microscope at about 125 × - 1250 × magnification with cross-polarized and transmitted light. Detailed core descriptions are given in (Pätzold and cruise participants, 1999). A Minolta CM - 2002^{TM} hand-held spectrophotometer was used to measure percent reflectance values of sediment color at 31 wavelength channels over the visible light range (400-700 nm). The digital reflectance data of the spectrophotome-

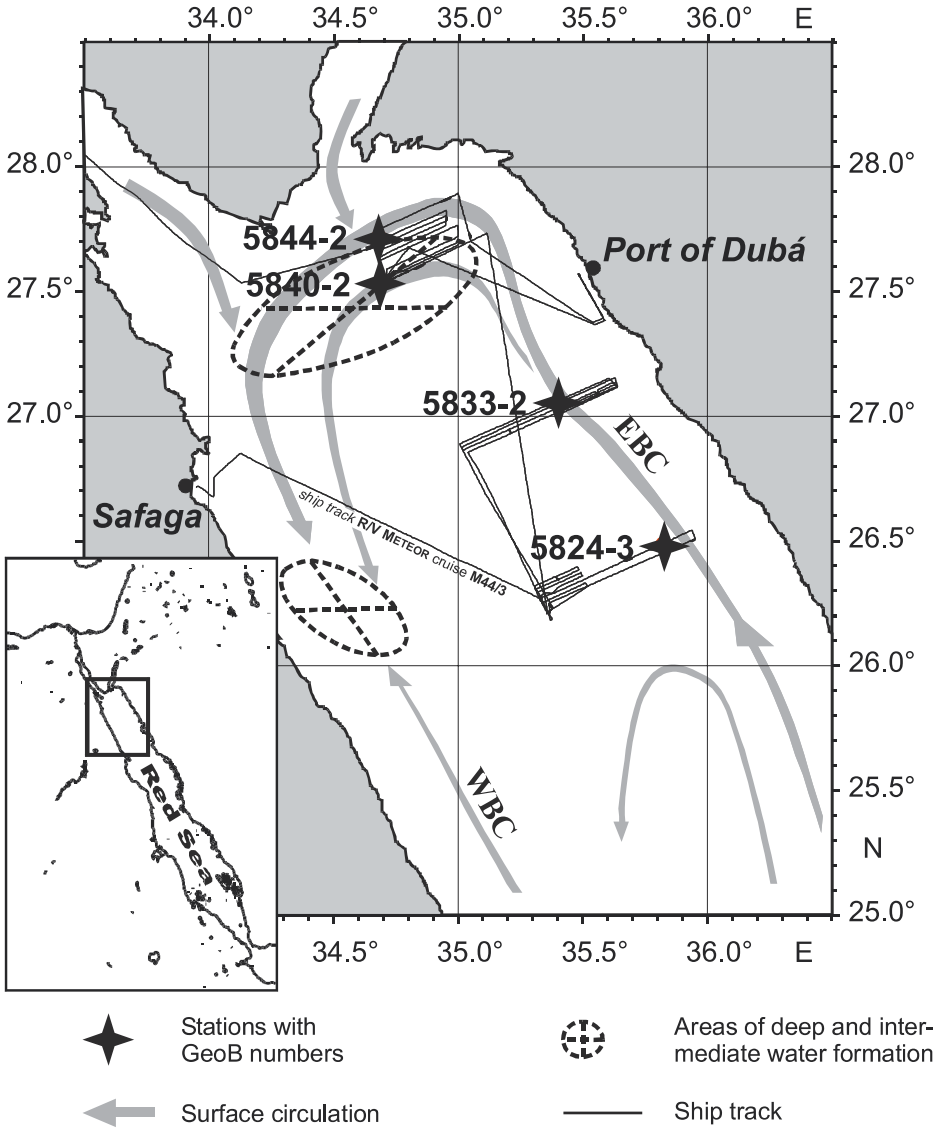

FIG. 1. Locations of sediment cores (black stars), ship track of R/V METEOR cruise M44/3, and schematic surface circulation pattern including key areas of deep water formation in the northern Red Sea (after, Eshel, 1997). WBS, Western Boundary Current; EBS, Eastern Boundary Current.

TABLE 1. List of investigated gravity cores retrieved during R/V METEOR cruise M44/3.

GeoB no.	Latitude ºN	Longitude ºE	Water depth (m)	Core length (cm)
5824-3	26º29.12′	35º49.50′	587 m	1016 cm
5833-2	27º03.17′	35º24.26′	628 m	1638 cm
5840-2	27º31.66′	34º41.24′	909 m	1630 cm
5844-2	27º42.81′	34º40.90′	963 m	1235 cm

ter readings were routinely obtained from the surface (measured in 0.5 or 1 cm steps) of the split cores (archive half).

X-Ray Fluorescence (XRF) Core Scanner and Multi Sensor Core Logger (MSCL)

Bulk-sediment chemistry was determined by means of profiling X-ray fluorescence (XRF; 1 cm resolution) using a newly developed XRF core-scanner (Jansen *et al*., 1998) (Fig. 2). By this method, chlorine and elements of higher atomic number are evaluated in terms of element intensities. Generally, Ca and Sr intensities correlate well with the carbonate content, whereas elements like Fe, Ti and K are related to siliciclastic components and vary directly with the terrigenous fraction of the sediment (Arz, 1998 and Jansen *et al*., 1998). An independent indicator for the terrigenous sediment input (*i.e*., ferromagnetic minerals) is the magnetic susceptibility measured with the MSCL.

Spectral Analysis

Spectral analyses of the data sets were performed with the AnalySeries software (Paillard *et al.*, 1996). We calculated the Blackman-Tukey power spectra (80% confidence level, high/low resolution) of the detrended and normalized data sets.

Results and Discussion

Sediment Composition

According to the macroscopic description and smear slide analysis, the sediments are moderately bioturbated, foraminifer bearing, olive gray to white nannofossil oozes, which contain variable amounts of terrigenous material (clay to sand). The profiling color reflectance values and especially the 700 nm wave length of the visual light spectra of the sediments from the northern Red Sea transects strongly reflect the compositional variations of the sediment through time. As described by Mix *et al.* (1992), but also in this particular case, light colors (high 700 nm reflectance) represent carbonate rich interglacial sediments and dark colors more terrigenous glacial sediments (Fig. 3).

Preliminary Stratigraphy and Sedimentation Rates

In Fig. 4ab we compare the color measurements (*i.e*., the 700 nm reflectance values) with the oxygen isotope record of a sediment core from the central Red Sea (Hemleben *et al*., 1996). First ^{14}C AMS dates on core GeoB 5844-2 (Table 2, Fig. 4a) and the overall correspondence (Fig. 4b) clearly demonstrates that sediment color is an adequate stratigraphic tool for sediment cores in the Red Sea area. According to the preliminary stratigraphies, the sedimentary records extend back to about 0.5 million years, comprising the last 6 glacial-interglacial cycles with sedimentation rates of 3.5 to 8 cm/ka. By comparing the age/depth relation of the investigated cores, a clear northward increase of the sedimentation rates can be observed (Fig. 5). Increasing sedimentation rates towards the north may document two major processes controlling sedimentation in the northern Red Sea. Firstly, terrigenous sedimentation could have been generally

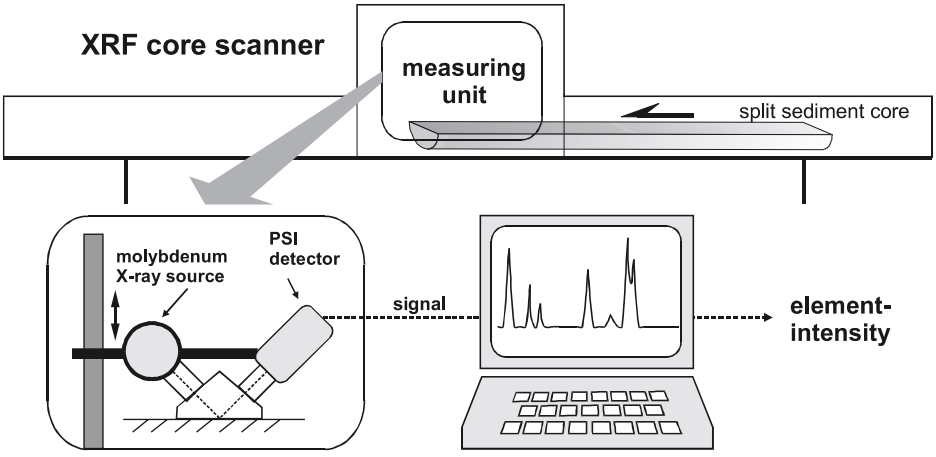

FIG. 2. Schematic illustration of the principal measurement units of the X-Ray Fluorescence core scanner developed at the Netherlands Institute for Sea Research (NIOZ) (Jansen *et al.,* 1998).

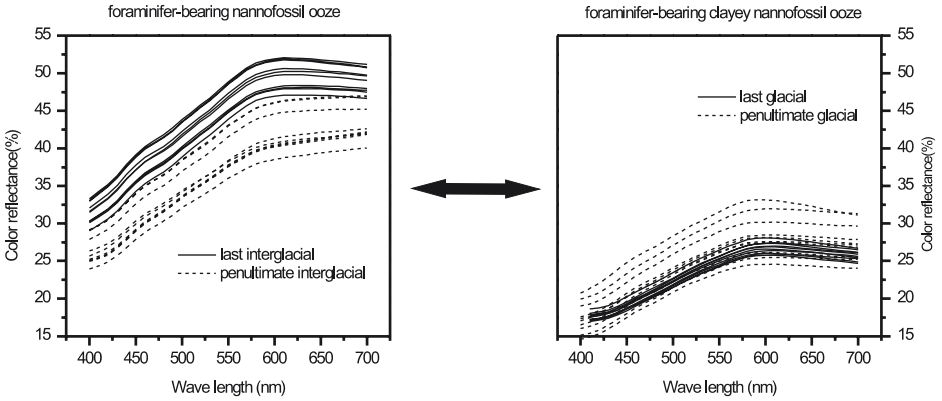

FIG. 3. Color reflection spectra of the visual light, measured with a Minolta CM - 2000^{TM} hand-held spectrophotometer, showing spectral characteristics of two different types of sediments: interglacial foraminifer-bearing nannofossil ooze and glacial foraminifer-bearing clayey nannofossil ooze.

TABLE 2. ^{14}C ages obtained by Accelerator Mass Spectrometry dating of monospecific samples in core GeoB 5844-2, performed at the Leibniz-Labor AMS facility in Kiel, Germany (Nadeau *et al.,* 1997). ^{14}C ages were reservoir corrected using the CALIB 4.3 calibration software (Stuiver and Reimer, 1993), considering a regional deviation from the global reservoir effect (ΔR) of ~ 100 years.

Lab.-ID	Core depth (cm)	Foram/Pteropod species	^{14}C AMS age (yr B.P.)	± Err (yr)	Calibrated age (cal. yr B.P.)
KIA11275	55	*G. sacculifer*	8525	55	8920
KIA11281	150	*Creseis acicula*	17030	90	19590
KIA11287	250	*Creseis virgula*	25110	205	28910
KIA11292	350	*G. bulloides*	36100	350	41090

higher in the north due to an elevated relief surrounding the Red Sea in its northern part and the year round dominating northerly winds and associated aeolian input. Secondly, continual deep mixing events (Cember, 1988; Felis *et al*., 1998 and Woelk & Quadfasel, 1996), probably associated with a nutrient redistribution into surface waters, could have increased primary production and biogenic accumulation towards the north. In order to assess and separate these different processes we briefly present and discuss the results obtained by the core logging methods.

The Proxies of Terrigenous Sediment Input

In Fig. 6 we show the magnetic susceptibility (MSCL) and the element intensities of Fe, Ti, and Mn (XRF-scanner) on gravity core GeoB 5840-2. According to their general distribution in terrigenous sediments, the records of Fe and Ti parallel each other, but their variations are of different magnitude. The glacial/interglacial pattern clearly dominates, with high values during glacial and low values during the interglacial periods. This generally agrees with color data and core description information. Magnetic susceptibility is also highly correlated with the Fe intensities (R = 0.67). Assuming that sediment composition is determined by the two major components, biogenic carbonate and terrigenous material, the input of terrigenous material increased during glacials at the expense of the carbonate accumulation. The main source of terrestrial material is probably the aeolian dust blown out from the surrounding desert areas. Today, dust storms and hazes frequently occur in the northern Red Sea area, especially in winter and spring, transporting lithogenic material to remote areas of the Red Sea (Middleton, 1986 and Pye, 1987). Increased input of aeolian dust during glacials may indicate a higher aridity and availability of material on the adjacent continent.

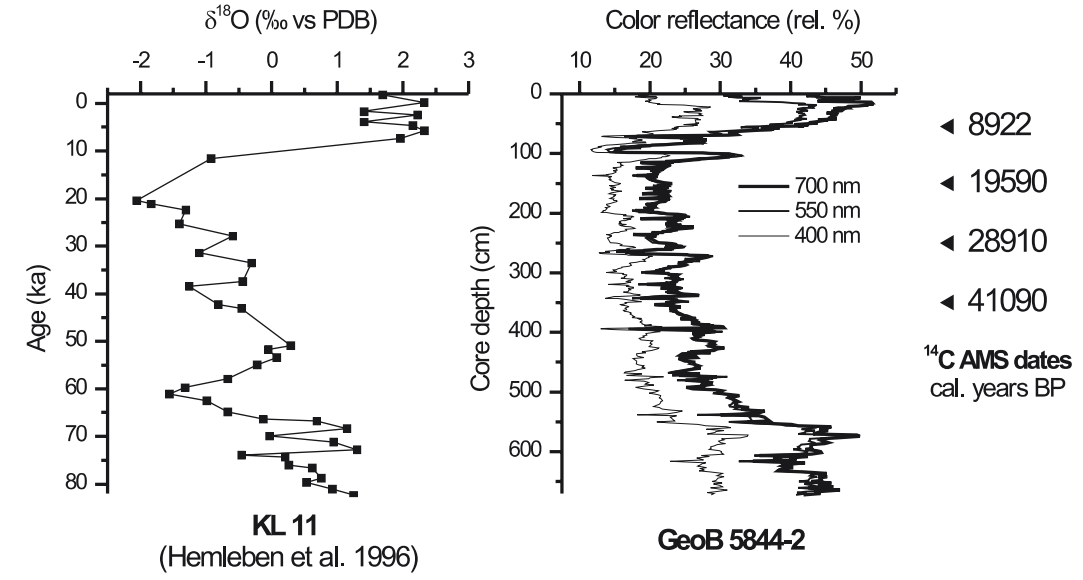

(A)

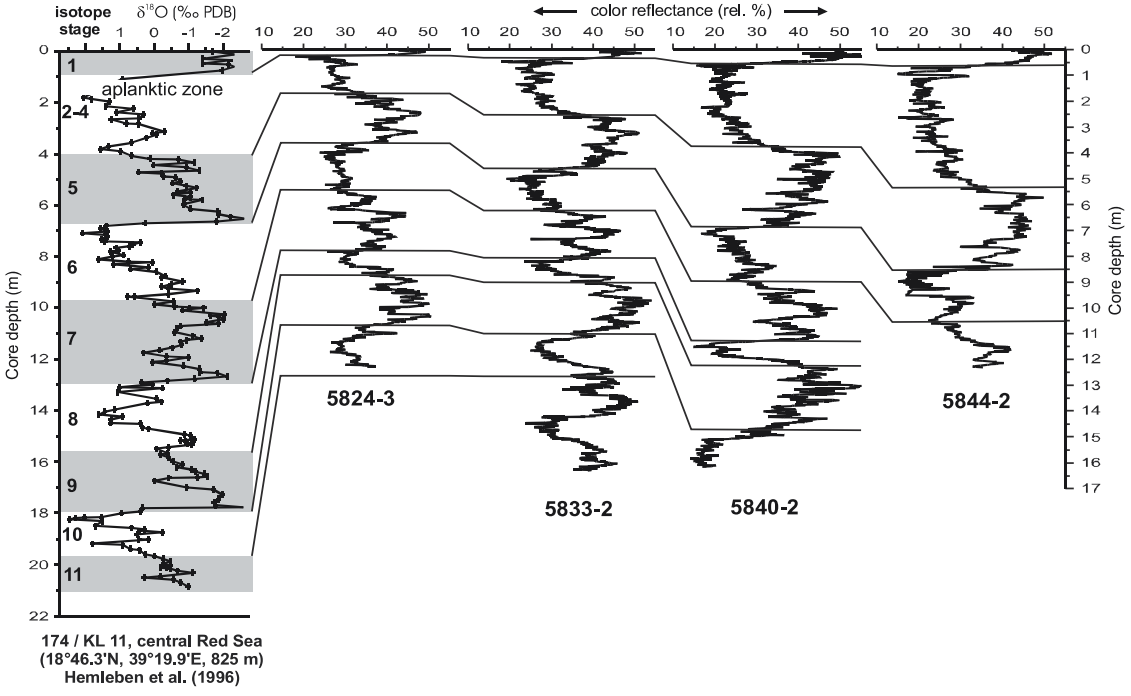

(B)

FIG. 4(A). Comparisons of the sediment color (light reflectance at 700, 550, and 400 nm wave length) of the ^{14}C AMS dated gravity core GeoB 5844-2 with the isotopic record of core KL 11 from the central Red Sea (Hemleben *et al*., 1996). (b) Comparisons of the sediment color (light reflectance at 700 nm wave length) of the investigated gravity cores listed in Table 1 with the isotopic record of core KL 11 from the central Red Sea (Hemleben *et al*., 1996).

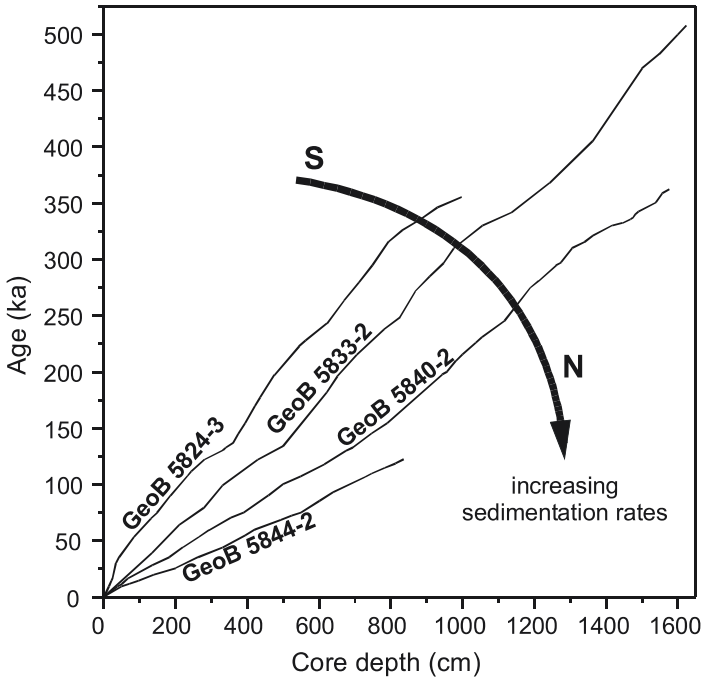

FIG. 5. Age-depth relation of the investigated cores based on detailed correlations with the stable oxygen isotope record from (Hemleben *et al*., 1996) and the SPECMAP stack (Imbrie *et al*., 1984). Our cores were stratigraphically linked to each other through the magnetic susceptibility signal. Note the increasing sedimentation rates to the North.

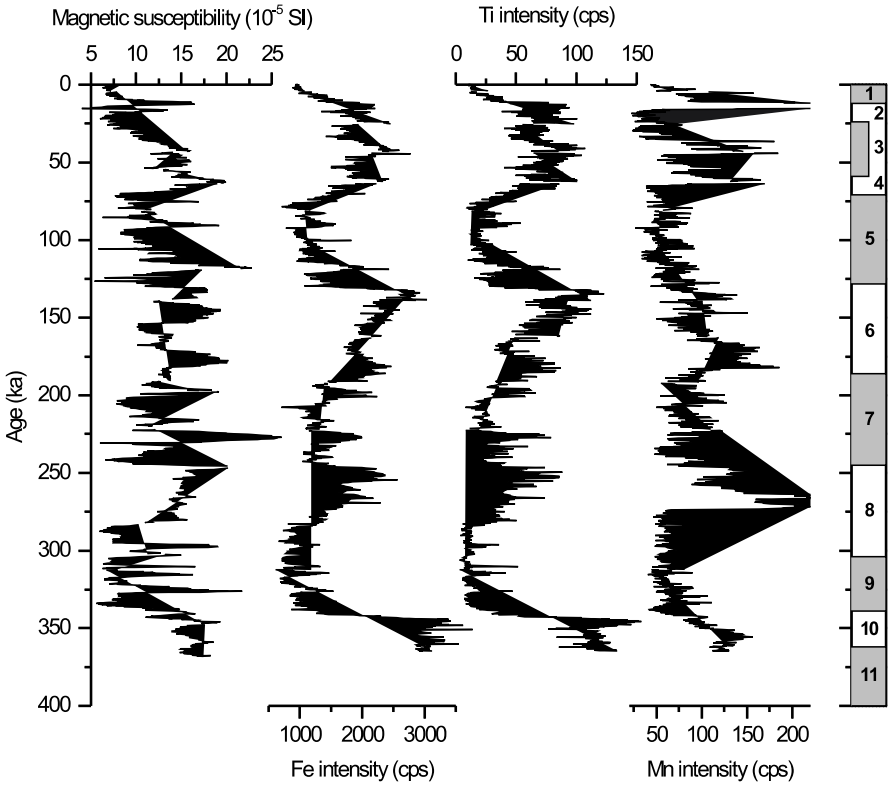

FIG. 6. Magnetic susceptibility and element intensities of Fe, Ti, and Mn for core GeoB 5840-2 plotted versus time. One the right-hand side the Marine Isotope Stages are shown (Imbrie *et al.,* 1984).

Various paleoclimatological studies already used the lithogenic input to the Gulf of Oman and the Arabian Sea as an indicator for aridity on the Arabian Peninsula. These studies suggest that during glacials generally more arid conditions prevailed and the input of terrigenous material was increased (*e.g.*, Clemens *et al*., 1996 and Clemens & Prell, 1990). Cross spectra between the SPECMAP record of global sea-level (Imbrie *et al*., 1984) and the intensity data of core GeoB 5840-2, used as a proxy for the terrigenous input, indicate highest spectral density and cross coherency at the prominent Milankovitch-periods of 100, 41 and 23 ka (Fig. 7). However, in the Fe record the precessional band is, in contrast to the SPECMAP spectrum, as dominant as the major eccentricity period. This might be interpreted as a significant contribution of the precession-controlled changes in the summer northwesterly wind intensity (related to the SW-monsoon) to the aeolian lithogenic transport in the area. Variability in the NNW-SSE gradient in the lithogenic input (Fe intensity difference of GeoB 5840-2 and GeoB 5824-3) is dominated by the precession and semi-precession periods (Fig. 8), a fact that is probably related to the continent proximity with reference to the main wind direction.

The Proxies of Marine Productivity

The Ca intensity as a measure for the Ca content in marine sediments is generally related to the carbonate content (Arz, 1998; Arz *et al*., 1999; Arz *et al*., 1998 and Jansen *et al*., 1998). By calibrating the Ca counts, based on a linear correlation with the actual carbonate content ($r^2 = 0.94$; Arz, 1998), we can express them in terms of carbonate content (Fig. 9). The carbonate content records in all investigated sediment cores describe a clear glacial/interglacial pattern, with high values during interglacials (~ 80 wt %) and low values during the glacial periods (20-40 wt %). This generally agrees with abundance patterns of planktonic foraminifera and coccolithophorids as previously reconstructed from Red Sea sediment cores (*e.g.*, Almogi-Labin *et al*., 1998; Geiselhart, 1998; Hemleben *et al*., 1996 and Winter *et al*., 1983). Much of the glacial/interglacial variability can be explained by sea-level driven changes in surface salinity and nutrient supply (*e.g.*, Almogi-Labin *et al*., 1998; Winter *et al*., 1983).

During interglacial sea-level high stands "normal" ocean water enters the Red Sea through the Street of Bab el Mandeb, continuously replacing the more saline surface waters of the northern Red Sea and creating more favorable growing conditions. During glacials the inflow of open ocean water is reduced, leading to increased surface salinities that restrict the occurrence of many planktonic organisms due to their reduced salinity tolerance. This process probably culminated during the Last Glacial Maximum (~18 ka), a period of maximum sea surface salinities (> 53‰), with a so-called aplanktic zone that can be observed in many sedi-

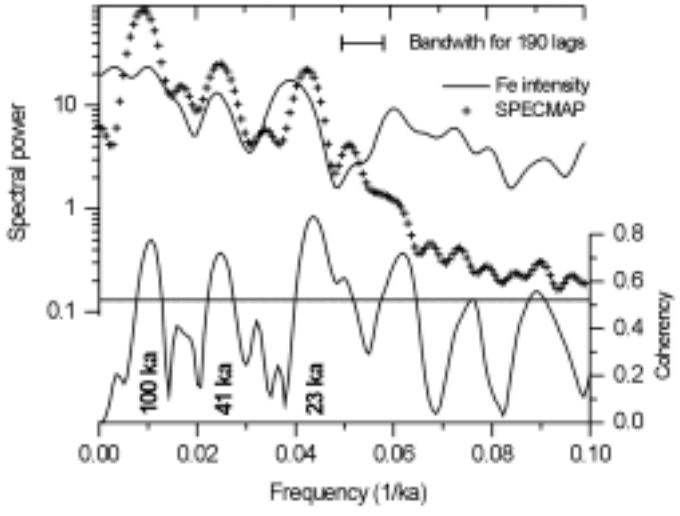

FIG. 7. Spectral density and cross-coherency of XRF-measured Fe intensities of core GeoB 5840-2 and the SPECMAP stack. Statistically significant coherence (80% level) is demonstrated over the major Milankovitch periods.

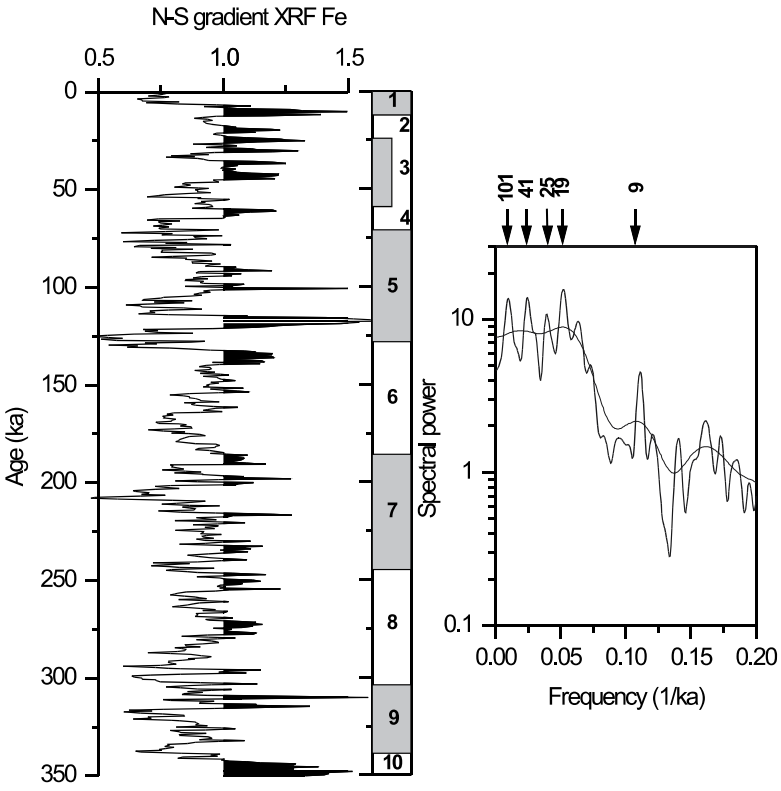

FIG. 8. Left) N-S gradient in Fe intensities calculated as difference between the Fe intensity records of cores GeoB 5840-2 and GeoB 5824-3, and (Right) high- and low-resolution spectral density of the Fe difference.

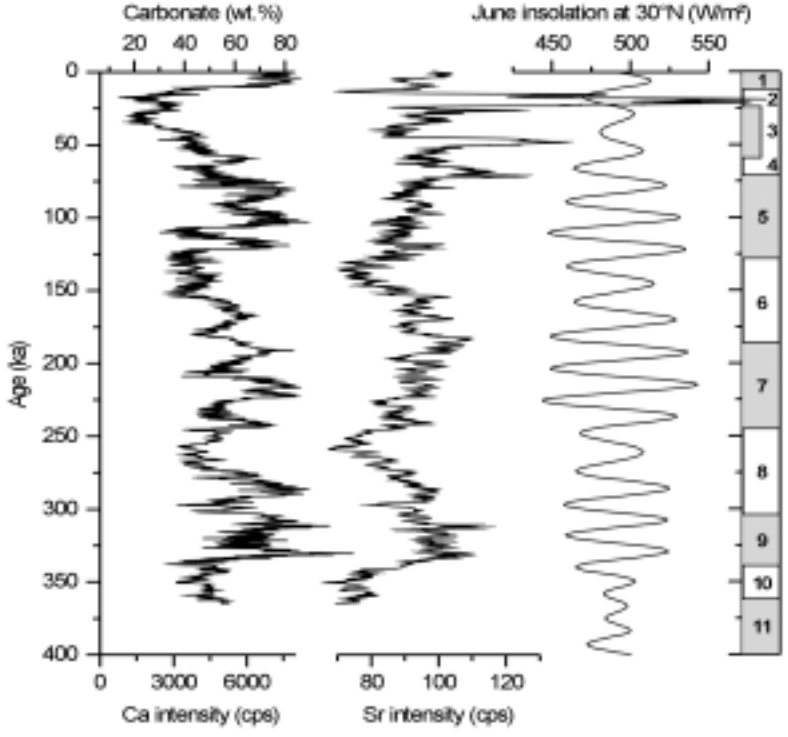

FIG. 9. XRF measured element intensities of Ca and Sr for core GeoB 5840-2 plotted versus time. Note the additional axis for the Ca record, were the linear relationship to the actual carbonate content of the sediment is indicated. One the right-hand side the June insolation at 30ºN and the Marine Isotope Stages (Imbrie *et al*., 1984) are plotted.

ment cores of the central and northern Red Sea (*e.g.*, Hemleben *et al.*, 1996).

Results on spectral analyses show that glacial/interglacial cycles are well recorded in the Ca intensity (Fig. 10). However, there is also a significant correspondence with summer insolation at 30ºN, mainly dominated by precessional cycles, which strongly suggest the influence of the monsoonal system on the carbonate production in the northern Red Sea. As suggested by Almogi-Labin *et al.* (1998), surface water stratification and therefore primary productivity could have varied with changing aridity in response to precession-controlled variations in the monsoonal system. Additionally, variations in the water exchange of the Red Sea with the Gulf of Aden, which are partially controlled by the monsoonal winds, could have been a possible source for variations in the nutrient distribution in the Red Sea.

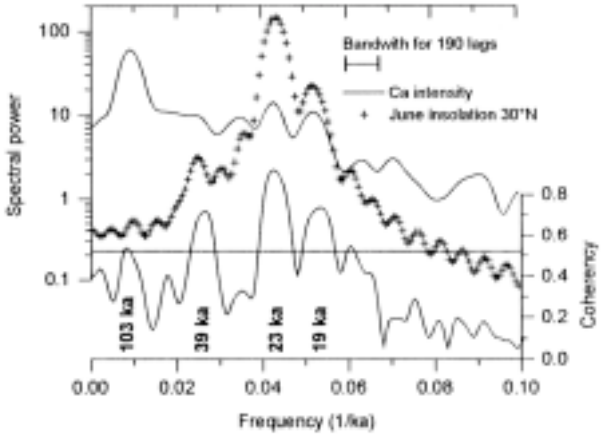

FIG. 10. Spectral density and cross-coherency of XRF-measured Ca intensities of core GeoB 5840-2 and the June insolation at 30ºN. Statistically significant coherence (80% level) is demonstrated over the 23-19 ka precession band.

Another element intensity, the Sr intensity, is plotted in Fig. 9. Sr is preferentially incorporated in aragonite and therefore may be related to the relative contribution of aragonitic pteropod shells to the carbonate content. Generally, the Sr intensity parallels the carbonate content, reflecting higher abundances of pteropods during interglacials. However, we know from the work of Almogi-Labin *et al.* (1998) that pteropod preservation was not constant over the last 400 ka and periods of repeated aragonite dissolution or secondary aragonite precipitation may have overprinted the Sr signal. Most prominent is the Sr-maximum during the LGM, when, of all planktonic fauna, only the salinity tolerant pteropod *Creseis acicula* survived the high surface salinities and inorganic aragonitic crusts were formed.

Besides the major Milankovitch periods, centennial to millennial scale variations occur in the Ca record, with dominant periodicities centered near 3.6 ka, 2 ka, and 1.5 ka (Fig. 11), which correspond to similar climate cycles known from the North Atlantic region (*e.g.*, Bond *et al.*, 1999). Deep-water formation in the northern Red Sea is partially initiated by deep mixing events (Eshel & Naik, 1997 and Woelk & Quadfasel, 1996). Today, these processes are related to extreme atmospheric events, leading subsequently to a vertical nutrient redistribution into the surface water and therefore to enhanced productivity. Such atmospheric deteriorations could originate from the North Atlantic region, changing their intensity and frequency over time.

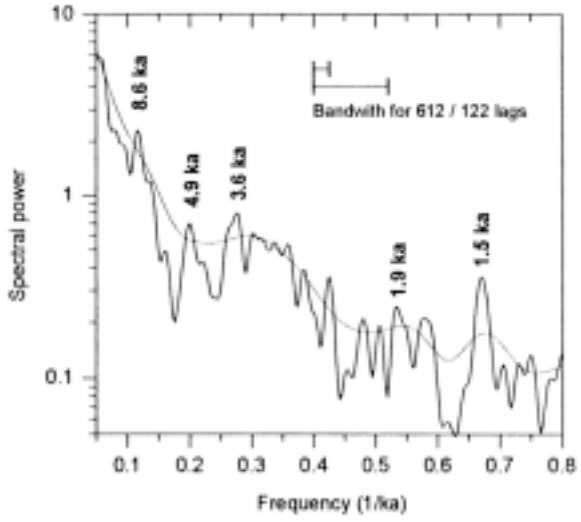

FIG. 11. High- and low-resolution spectral density of the Ca record of core GeoB 5844-2.

Conclusions

Profiling, high-resolution scanning methods (color, MSCL, XRF) allow a semi-quantitative characterization of the sediment cores and provide powerful tools for stratigraphic purposes and paleoenvironmental interpretations. We investigated four gravity cores on a N-S transect in the northern Red Sea. Logging results show a consistent picture of late Quaternary changes in terrigenous sediment

input and marine carbonate production in the study area. Our Red Sea paleoenvironmental records are predominantly controlled by the global, glacial/ interglacial climatic cycles and the associated glacio-eustatic sea level changes. However, a strong periodic variability in the range of the precessional forcing band suggests a direct link to variations in the African/Asian monsoonal system.

For a more detailed examination of the variability in all the proxies, the stratigraphy will have to be significantly improved by additional ^{14}C AMS dating and stable oxygen isotope measurements on calcareous planktonic organisms. With a more reliable stratigraphy, time series analyses will become more consistent and will allow a detailed comparison to climate records from other parts of the world. Additionally, stable isotope measurements on different planktonic and benthonic organisms, as well as faunal investigations and independent determinations of paleo sea surface temperatures will enforce future paleoceanographic reconstructions.

Acknowledgements

We gratefully acknowledge the assistance of Captain Bülow and his crew, who substantially contributed to the overall scientific success of this cruise. We also acknowledge the generous grant of permission for conducting research in the territorial waters of the Kingdom of Saudi Arabia with the German research vessel METEOR in March/April 1999. The work was funded by the Deutsche Forschungsgemeinschaft grant no. PA 492/4-1.

References

Almogi-Labin, A., Hemleben, C. and **Meischner, D.** (1998) Carbonate preservation and climatic changes in the central Red Sea during the last 380 kyr as recorded by pteropods, *Mar. Micropal.*, **33:** 87-107.

Arz, H. (1998) *Dokumentation von kurzfristigen Klimaschwankungen des Spätquartärs in Sedimenten des Westlichen Äquatorialen Atlantiks,* PhD Thesis, Berichte aus dem Fachbereich Geowissenschaften der Universität Bremen 124: 115 p.

Arz, H.W., Pätzold, J. and **Wefer, G.** (1998) Correlated millennial-scale changes in surface hydrography and terrigenous sediment yield inferred from last-glacial marine deposits off northeastern Brazil, *Quat. Res,*. **50:** 157-166.

Arz, H., Pätzold, J. and **Wefer, G.** (1999) Climatic changes during the last deglaciation recorded in sediment cores from the Northeast Brazilian Continental Margin, *Geo Mar. Let.,* **19:** 209-218.

Barry, R.G. and **Chorley, R.J.** (1998) *Atmosphere, Weather and Climate,* Routeledge, London, 409 p.

Bond, G.C., Showers, W., Elliot, M., Evans, M., Lotti, R., Hajdas, I., Bonani, G. and **Johnson, J.** (1999) The North Atlantic's 1-2 kyr climate rhythm: relation to Heinrich Events, Dansgaard/Oeschger Cycles and the Little Ice Age, *In: Mechanisms of Global Climate Change at Millennial Time Scales,* P. U. Clark, R. S. Webb, and L. D. Keigwin, (Eds.), AGU, Washington, pp. 35-58.

Brachert, T.C. (1995) Production of cryptocrystalline carbonate in an extreme environment: The deep glacial Red Sea, *Veröffentlichungen des Luxemburger geologischen Dienstes,* **29:** 13.

Cember, R.P. (1988) On the sources, formation and circulation of Red Sea deep water, *J. Geophys. Res.,* **93:** 8175-8191.

Clemens, S.C. and **Prell, W.L.** (1990) Late Pleistocene variability of Arabian Sea summer monsoon winds and continental aridity: eolian records from the lithogenic component of deep-sea sediments, *Paleoceanogr.,* **5:** 109-145.

Clemens, S.C., Murray, D.W. and **Prell, W.L.** (1996) Nonstationary phase of the Plio-Pleistocene Asian monsoon, *Science,* **274:** 943-948.

Edwards, F.J. (1986) Climate and Oceanography, In: *Red Sea,* (A. J. a. S. M. H. Edwards, Ed.), 45-69.

Eshel, G., Cane, M.A. and **Blumenthal, M.B.** (1994) Modes of subsurface, intermediate, and deep water renewal in the Red Sea, *J. Geophys. Res.,* **99:** 15941-15952.

Eshel, G. and **Naik, N H.** (1997) Climatological coastal jet collision, intermediate water formation and the general circulation of the Red Sea, *J. Phys. Oceanogr.,* **27:** 1233-1257.

Felis, T., Pätzold, J., Loya, Y. and **Wefer, G.** (1998) Vertical water mass mixing and plankton blooms recorded in skeletal stable carbon isotopes of a Red Sea coral, *J. Geophys. Res.,* **103:** 30731-30739.

Geiselhart, S. (1998) *Late Quaternary Paleoceanographic and Paleoclimatologic History of the Red Sea during the Last 380,000 Years: Evidence from Stable Isotopes and Faunal Assemblages,* Ph.D. Thesis, Institut und Museum für Geologie und Paläontologie der Universität Tübingen, 87 p.

Gvirtzman, G., Kronfeld, J. and **Buchbinder, B.** (1992) Dated coral reefs of southern Sinai (Red Sea) and their implication to late Quaternary sea levels, *Mar. Geol.,* **108:** 29-37.

Hemleben, C., Meischner, D., Zahn, R., Almogi-Labin, A., Erlenkeuser, H. and **Hiller, B.** (1996) Three hundred eighty thousand year long stable isotope and faunal records from the Red Sea: Influence of global sea level change on hydrography, *Paleoceanogr.,* **11:** 147-156.

Imbrie, J., Hays, J.D., Martinson, D.G., McIntyre, A., Mix, A.C., Morley, J.J., Pisias, N.G., Prell, W. L. and **Shackleton, N. J.** (1984) The orbital theory of Pleistocene climate: support from a revised chronology of the marine $\delta^{18}O$ record, *In: Milankovitch and Climate,* A. L. Berger, J. Imbrie, J. D. Hays, J. Kukl, and J. Saltz-

man (Eds.), 269-305, Reidel Publishing Company, Hingham.

Jansen, J.H.F., Van der Gaast, S.J., Koster, B. and **Vaars, A.** (1998) CORTEX, a shipboard XRF-scanner for element analyses in split sediment cores, *Mar. Geol.,* **151:** 143-153.

Locke, S.M. and **Thunell, R.C.** (1988) Paleoceanographic record of the last glacial/ interglacial cycle in the Red Sea and Gulf of Aden, *Geochemical Measures of Modern and Ancient Oceanographic Processes,* **64:** 163-187.

Middleton, N.J. (1986) Dust storms in the Middle East, *J. Arid Env.*, **10:** 83-96.

Milliman, J.D., Ross, D.A. and **Ku, I.L.** (1969) Precipitation and lithification of deep-sea carbonates in the Red Sea, *J. Sed. Petrol.,* **39:** 724-736.

Mix, A.C., Rugh, W., Pisias, N.G. and **Veirs, S.** (1992) Color reflectance spectroscopy: A tool for rapid characterization of deep-sea sediment, *In: Proceedings of the Ocean Drilling Project,* Initial Report, (I. Mayer, N. G. Pisias, and T. Janecek *et al*. (Eds.), pp. 67-77.

Morcos, S.A. (1970) Physical and chemical oceanography of the Red Sea, Oceanogr., *Mar. Biol. Annu. Rev.,* **8:** 73-202.

Nadeau, M.J., Schleicher, M., Grootes, P.M., Erlenkeuser, H., Gottdang, A., Mous, D.J.W., Sarnthein, J.M. and **Willkomm, H.** (1997) The Leibniz-Labor AMS facility at the Christian-Albrechts University, Kiel, Germany, *Nuc. Instr. Meth. Phys. Res.,* B **123:** 22-30.

Paillard, D., Labeyrie, L. and **Yiou, P.** (1996) Macintosh program performs time-series analysis, *Eos Trans.,* **AGU 77:** 379.

Patzert, W.C. (1972). Seasonal reversal in Red Sea circulation, *In: Symposium de l'Association Internationale des Sciences Physique de l'ocean* (I.A.P.S.O.) Paris, pp. 55-89.

Pätzold, J. and **cruise participants** (1999) *Report and Preliminary Results of R/V Meteor Cruise 44/3,* Department of Geosciences, University Bremen, Bremen, 69 p.

Pye, K. (1987) *Aeolian Dust and Dust Deposits*, Academic Press Inc., London, 334 p.

Stuiver, M. and **Reimer, P.J.** (1993) Extended ^{14}C data base and revised CALIB 3.0 ^{14}C age calibration program, *Radiocarbon,* **35:** 215-230.

Tragou, E. and **Garrett, C.** (1997) The shallow thermohaline circulation of the Red Sea, *Deep-Sea Res.,* **44:** 1355-1376.

Winter, A., Almogi-Labin, A., Erez, Y., Halicz, E., Luz, B. and **Reiss, Z.** (1983) Salinity tolerance of marine organisms deduced from Red Sea quaternary record, *Mar. Geol.,* **53:** 1417-1422.

Woelk, S. and **Quadfasel, D.** (1996) Reneval of deep water in the Red Sea during 1982-1987, *J. Geophys. Res.,* **101:** 18155-18165.

السجل المناخي لأواخر الدهر الرابع من شمال البحر الأحمر: نتائج من المقاطع اللبيبة التثاقلية المسحوبة خلال الرحلة العلمية (R/V Meteor cruise M44/3)

هيلج آرز[١]، وجورجين باتزولد[١]، ومصطفى معمر[٢]، و أورسولا روهى[١]

[١]*جامعة بريمن – ألمانيا* و [٢]*كلية علوم البحار، جامعة الملك عبد العزيز، جدة – المملكة العربية السعودية*

المستخلص. تم عرض دقة عالية لسجل المناخ القديم للبيئة البحرية الذي تم الحصول عليه من المقاطع اللبيبة للرسوبيات المسحوبة من ثلاثة محاور ممتدة من الشاطئ السعودي إلى المحور الأوسط للبحر الأحمر خلال الرحلة العلمية (R/V Meteor cruise M44/3) في ربيع ١٩٩٩م . بسبب انحصاره بالصحاري المحيطة به ، تعرض شمال البحر الأحمر لتقلبات إقيانوغرافية شديدة في الماضي ، نتج عنها تكبير وتضخيم لدلائل المناخ القديم في الرسوبيات البحرية . الترسب المستمر لرواسب البيئة القارية المزرية بالرياح يوفر دقة زمنية عالية للتغير في جفاف المناطق القارية المتاخمة .

هذه التغيرات موثقة بمؤشرات ودلائل مستقلة ، مثل التغير في التركيب الكيميائي للرسوبيات الكلية (Fe- and Ti-content) المقدرة بقياسات XRF وقابلية التمغنط . ويتوافق مع ذلك ، التغير في البيئة البحرية المنعكس بالتغير في محتوى الكربونات Ca- and Sr intensities . هذا البحث يقدم دليلاً على وجود ترابط قوي لكل من التغير في جفاف الشرق الأدنى والتغير في الظروف البيئية البحرية القديمة في شمال البحر الأحمر من جهة ، والتغير في المناخ العالمي والتغير في مستوى سطح البحر من جهة أخرى ، وكذلك الاختلاف في نظام الرياح الموسمية .